Climbing, falling, and jamming during ant locomotion in confined environments

Nick Gravish[a,1], Daria Monaenkova[a], Michael A. D. Goodisman[b], and Daniel I. Goldman[a,1]

[a]School of Physics and [b]School of Biology, Georgia Institute of Technology, Atlanta, GA 30332

Edited by David B. Wake, University of California, Berkeley, CA, and approved April 16, 2013 (received for review February 5, 2013)

Locomotion emerges from effective interactions of an individual with its environment. Principles of biological terrestrial locomotion have been discovered on unconfined vertical and horizontal substrates. However, a diversity of organisms construct, inhabit, and move within confined spaces. Such animals are faced with locomotor challenges including limited limb range of motion, crowding, and visual sensory deprivation. Little is known about how these organisms accomplish their locomotor tasks, and such environments challenge human-made devices. To gain insight into how animals move within confined spaces, we study the locomotion of the fire ant *Solenopsis invicta*, which constructs subterranean tunnel networks (nests). Laboratory experiments reveal that ants construct tunnels with diameter, D, comparable to body length, L = 3.5 ± 0.5 mm. Ants can move rapidly (> 9 bodylengths per s) within these environments; their tunnels allow for effective limb, body, and antennae interaction with walls, which facilitate rapid slip-recovery during ascending and descending climbs. To examine the limits of slip-recovery in artificial tunnels, we perform perturbations consisting of rapid downward accelerations of the tunnels, which induce falls. Below a critical tunnel diameter, D_s = 1.31 ± 0.02 L, falls are always arrested through rapid interaction of appendages and antennae with tunnel walls to jam the falls. D_s is comparable to the size of incipient nest tunnels (D = 1.06 ± 0.23 L), supporting our hypothesis that fire ants construct environments that simplify their control task when moving through the nest, likely without need for rapid nervous system intervention.

animal locomotion | extended phenotype | locomotion control | social insect | stability

Terrestrial animals and increasingly robots must move in diverse and complex environments, including running across flat landscapes (1), swimming in sand (2), climbing rough or smooth vertical surfaces (3), and squirming through cracks (4). The bulk of discoveries of locomotor behaviors and control strategies have been made by challenging animals in the laboratory in simplified environments that are typically featureless, flat, and unconfined (5). Such simplifications have allowed discovery of general principles in locomotor modes of walking, running, and climbing (6–9). Recent studies have generated appreciation for the importance of mechanical interactions with the environment, and through biological experiment (10) and robot modeling (11, 12) have demonstrated that stable and robust movement can emerge as a result of appropriately tuned dynamics of limb–ground interaction (13, 14). For example, rapid perturbations to locomotion may be corrected by so-called "preflexes" (15) in which mechanical design of the limb and appropriate kinematics enable rapid recovery from perturbation (6, 8, 10). However, typical substrates that legged locomotors contend with differ in orientation, can deform in response to foot/body contact (1, 11), and are rough on multiple size scales (16, 17); little is known about how organisms effectively use limb/body–substrate interactions in such environments. Practically, we expect that discovery of such principles can lead to advances of robotic devices that must operate in complex conditions; such devices often suffer performance loss in natural environments (11).

In particular, the role of confinement is relatively unexplored in locomotor performance and behavior. Many subterranean-dwelling organisms live and move within confined spaces in their environments (18, 19). The morphology (20, 21), energetic costs (22–25), and genetic basis (26, 27) for creating subterranean burrows and nests, which are examples of the "extended phenotype" (28), have been studied across a diversity of organisms. However, the constraints on locomotion of individuals and groups inhabiting these environments are largely unexplored (29). Rapid locomotion within the confines of a subterranean nest is essential for inhabitants to escape or respond to predators (18, 30), evacuate during flooding (31), or transport resources and information effectively (30). However, lack of vision (18, 19, 32), limited limb mobility (18), and excessive crowding among individuals (33) would seemingly challenge efforts at rapid locomotion within confined environments. Thus, we seek to understand how such environments influence the mobility and stability of animals moving within them.

Ants are excellent organisms with which to study confined locomotion. Many ant species construct large underground nests through the excavation of soil (34). Nest shape and size—in addition to ant shape and size—varies widely across species but typically consists of vertical tunnels that connect larger chambers used for food storage and brood rearing (21, 34). A majority of an ant colony worker's life is spent below the surface within the nest—tending to brood or performing routine nest maintenance—and only near the end of life do worker ants forage above surface (34–37). The evolutionary pressure of subterranean life has led to several adaptations among ants such as partial or complete loss of vision in some species (38, 39) and long-range acoustic (40–42) and chemical communication systems (38, 43, 44). However, almost nothing is known about how ants move through their confined nest environments.

We hypothesize that ants have developed strategies and adaptations for rapid movement within nests, particularly during crucial times such as nest reconstruction or evacuation. A species that frequently must contend with such events is the red imported fire ant (*Solenopsis invicta*). Fire ants originate from the Pantanal wetlands in South America, which are subject to seasonal rains and flooding (37). Fire ant colonies construct large and relatively complex subterranean nests (37) that can be up to 2 m deep and contain greater than 50 m in length of tunnels (45). As an invasive species in the Southern United States, fire ants have demonstrated proficiency at constructing nests within a wide range of soil conditions (37). Construction of such large nests demands the ability to move repeatedly and stably within the nest confines while transporting soil.

Author contributions: N.G., M.A.D.G., and D.I.G. designed research; N.G. and D.M. performed research; N.G. and D.M. analyzed data; and N.G., D.M., M.A.D.G., and D.I.G. wrote the paper.

The authors declare no conflict of interest.

This article is a PNAS Direct Submission.

[1]To whom correspondence may be addressed. E-mail: nick.gravish@gmail.com or daniel.goldman@physics.gatech.edu.

This article contains supporting information online at www.pnas.org/lookup/suppl/doi:10.1073/pnas.1302428110/-/DCSupplemental.

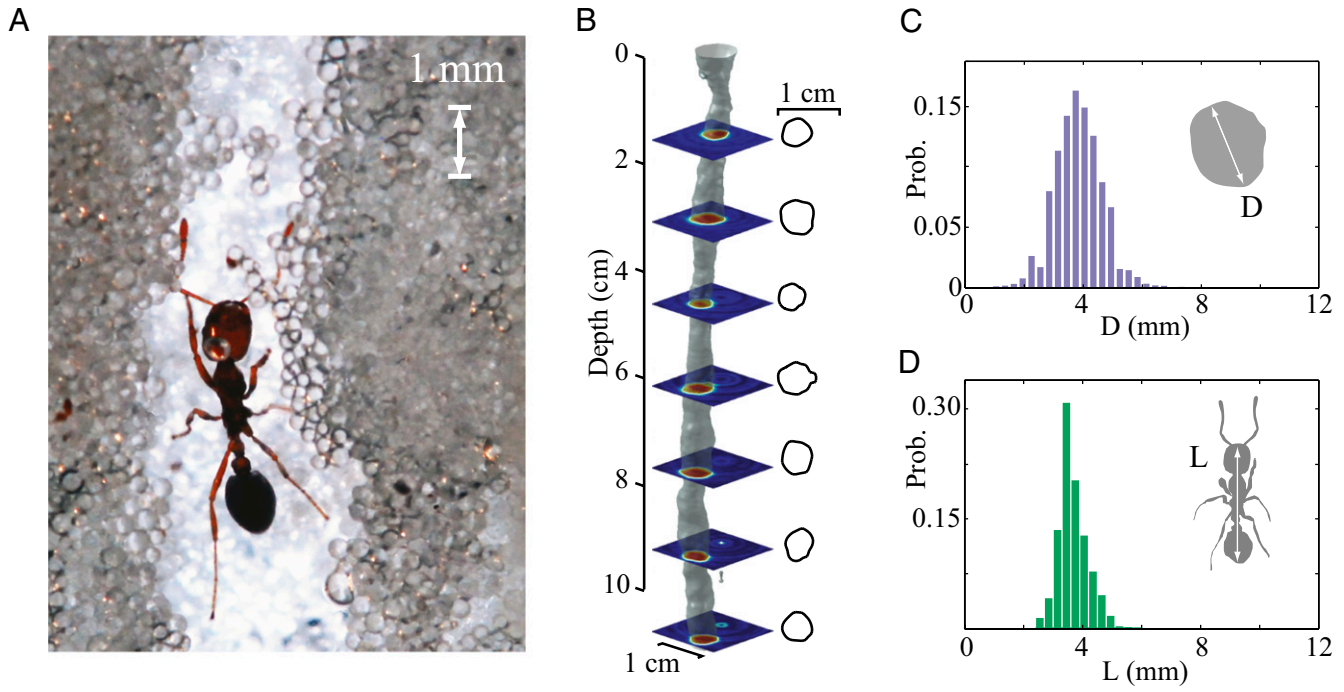

Fig. 1. Fire ants create and move through subterranean tunnels (Photo credit: Laura Danielle Wagner). (*A*) Image shows fire ant worker climbing within an ant-constructed tunnel against a clear glass pane. (*B*) X-ray CT scan reconstruction of a fire ant tunnel segment. (*C*) Probability distribution of tunnel cross-sectional diameter, D. In *A*–*C*, the substrate consists of wetted 250 micron approximately spherical glass particles. (*D*) Probability distribution of ant body length, L (measured from head to gaster), in laboratory climbing experiments.

In this article we seek to identify principles of locomotion within confined environments that challenge animals with a different set of locomotive constraints than in above-ground study. We investigate the effects of subterranean confinement (tunnel diameter) on the mobility and stability of the fire ant (*S. invicta*). We show that climbing in confined environments is a robust mode of high-speed locomotion, in which slips, falls, and frequent collisions with the environment do not necessarily prevent high-speed ascent and descent. We also demonstrate an unusual stabilizing response of fire ants when dislodged from the tunnel wall—the use of antennae as limb-like appendages to arrest and jam falls. Overall, we find that stable locomotion within subterranean environments is a function of the local tunnel morphology within which the organisms move. We hypothesize that the principle of off-loading locomotor control to the environment can be used by animals in confined environments and can inspire the next generation of mobile robots.

Results and Discussion

Shape and Form of Excavated Fire Ant Tunnels. To examine the interaction of fire ants with the tunnels that they constructed, we first measured the size and shape of nest tunnels excavated by fire ant workers (body length L = 0.35 ± 0.05, n = 2,611 measurements) in three-dimensions in a laboratory experiment using an X-ray computed tomography (CT) system (Fig. 1 and Fig. S1). We allowed isolated groups of fire ant workers to excavate tunnels within an 8 cm diameter, and 12 cm deep, cylindrical volume of laboratory soil (wet approximately spherical glass particles, see below) over the course of 20 h. The tunnels were roughly circular in cross-section (Fig. 1*B*, Fig. S2, and *SI Text*), and the effective cross-sectional diameter (*SI Text*) within the tunnels was D = 3.7 ± 0.8 mm (n = 2,262 observations from 10 experiments).

To determine if the soil substrate had an effect on tunnel shape and size, we repeated this experiment using different substrate combinations of particle diameter (50, 210, and 595 μm; See Table S1 for polydispersity) and soil moisture content (1%, 3%, 5%, 10%, 15%, 18%, and 20% by mass). We challenged worker groups from eight separate colonies to excavate tunnels in each substrate combination and collected 168 separate X-ray CT tunnel excavation observations (Fig. S3). We found a significant effect of both particle diameter ($F_{2,136}$ = 10.48, P < 0.0001) and soil moisture content ($F_{6,136}$ = 5.38, P < 0.0001) on excavated tunnel depth, indicating that substrate had a strong effect on digging proficiency. Soil moisture content had a nonlinear effect on tunnel depth. Tunnel depth was small at low soil moisture and rose to a maximum at intermediate soil moisture contents of 10–15%, above which tunnel depth decreased again at high soil moisture (*SI Text*).

Importantly, however, we found no significant effect of soil moisture ($F_{6,106}$ = 1.06, P = 0.39), particle diameter ($F_{2,106}$ = 1.56, P = 0.21), or the interaction of moisture and particle size ($F_{12,106}$ = 1.47, P = 0.15) on the tunnel diameter (*SI Methods*). Moreover, tunnels constructed in the laboratory and observed in X-ray CT were similar in diameter to tunnels found in natural fire ant nest mounds (4.4 mm) (46), nest entranceways (3–4 mm) (45), and incipient nests (3.1 ± 0.1 mm) (47), although tunnels deeper within natural nests may be larger in size (6.0 ± 3.0 mm) (46). Our results demonstrate that during tunnel founding, fire ants show a relatively fixed behavioral program by building tunnels of approximately the same diameter in a variety of conditions. This suggests that the diameter of the tunnel could be important in fire ant locomotion.

Tunnel Size Effects on the Biomechanics of Confined Climbing. To investigate the biomechanics of locomotion within tunnels, we monitored fire ants climbing within ant-constructed tunnels within Quasi-2D arenas (Fig. 1*A* and Movies S1–S3) and smooth cylindrical glass tubes (Fig. 2 *A* and *B*). We tracked the position of ascending and descending ants freely trafficking between

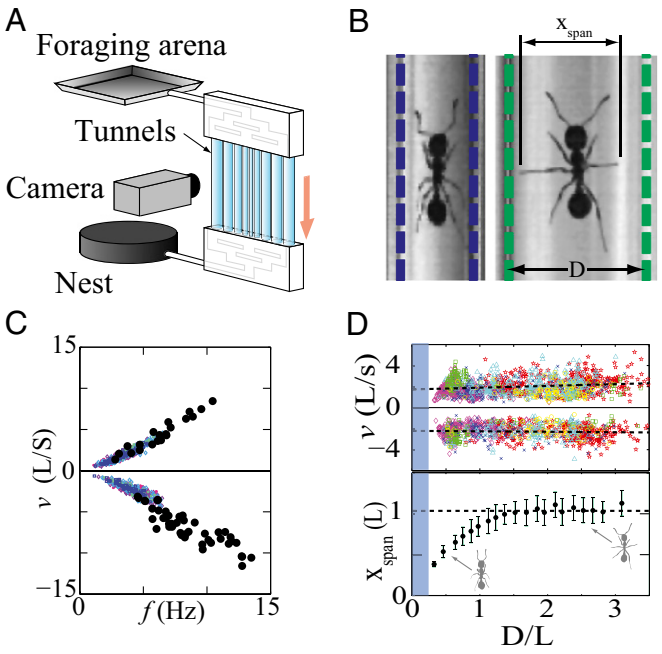

Fig. 2. Climbing posture and antennae use in glass tunnels. (*A*) Schematic of climbing biomechanics experiment. (*B*) Posture of ascending ant in a 2 mm diameter tunnel (*Left*; D = 0.60 L) and in a 6 mm diameter tunnel (*Right*; D = 1.36 L). Right image shows posture variable, x_{span}, measured in experiment. (*C*) Stride frequency and speed relationship for glass tunnels (colored points) and ant-created tunnels (filled black circles). (*D*, *Upper*) Speed versus D/L. Color indicates colony. Dashed lines are linear fits described in the text. Blue box indicates the minimum predicted tunnel diameter in which an ant could fit. (*D*, *Lower*) Lateral limb span (mean ± SD) as a function of normalized tunnel diameter. Dashed line indicates constant limb span of x_{span} = 1.04 ± 0.14 L independent of tunnel diameter.

a foraging arena and nest through glass tubes of diameters, D = 1.0–9.0 mm (in increments of 1 mm). We will refer to these glass tubes as "glass tunnels."

We found that ants rapidly ascended (2.0 ± 0.8 L·s^{-1}, n = 1,621 ants) and descended (2.3 ± 0.7 L·s^{-1}, n = 990 ants) in the glass tunnels (Figs. S4 and S5). The kinematic relationship between stride frequency and speed (Fig. 2*C*) was fit by the function $v = ax^2 + bx$ for both the ascending (a = 0.039 ± 0.003 L·s; b = 0.41 ± 0.01 L) and descending (a = –0.018 ± 0.005 L·s; b = –0.49 ± 0.02 L) climbs (Figs. S6 and S7). The speed–frequency relationship of ascent did not significantly differ among the ant-constructed tunnels and the glass tunnels of diameters, D = 0.3–0.4 mm (comparable to that of the self-constructed tunnels; $F_{2,361}$ = 1.8150, P = 0.1643). We did, however, find a small but significant difference in functional form of the speed–frequency relationship during descent ($F_{2,252}$ = 113.9, P < 0.001). To test maximal performance within ant-constructed tunnels, we induced an alarm response among the colony by exhaling into the tunnel entrance. Within ant-constructed tunnels, ants rapidly descended (6.9 ± 2.1 L·s^{-1}; n = 21) and ascended (4.1 ± 1.8 L·s^{-1}; n = 45) at speeds greater than observed in the glass tunnels and surprisingly were able to move at speeds greater than 9 L·s^{-1} within the confined, simulated nest environment.

Tunnel diameter had a weak but significant effect on ascending speed (Fig. 2*D*, *Upper*), as a function of D/L [v = m(D/L)+b; F test for nonzero slope, $F_{1,1619}$ = 63.132, P < 0.001; m = 0.17 ± 0.04 L^2·D^{-1}·s^{-1}, b = 1.73 ± 0.07 L·s^{-1}]. During descent in tunnels, D/L did not have a significant effect on speed (F test for nonzero slope, $F_{1,988}$ = 2.740, P = 0.10). We thus hypothesized that the minimum tunnel diameter through which an ant can move is slightly larger than the animal's head width. Fire ant head width is 0.24 ± 0.01 L (48), and this sets the lower limit of the range of observable D/L values (shaded blue box Fig. 2*D*). Both ascending and descending speeds near this lower limit (D/L < 0.5) sharply decreased (Fig. 2*D*, *Upper*), suggesting that only in the case of extreme confinement would we observe a strong effect of tunnel diameter on ascending or descending velocity. Overall, this suggests that ants move at a near constant upward and downward speed, over a wide range of tunnel sizes, while freely trafficking within the nest.

Tunnel diameter had a significant influence on climbing posture (Fig. 2*D*, *Lower*). Ants exhibited one of two stereotyped climbing postures: (*i*) within glass tunnels of D > L, ants adopted a sprawled posture in which midlimbs were extended laterally away from the body (Fig. 2*B*, *Right*), and (*ii*) within glass tunnels of D < L, midlimbs were bent and pointed posteriorly (Fig. 2*B*, *Left*). We determined the critical tunnel diameter at which this postural transition occurred by fitting the function $x_{span} = \begin{cases} k\left(\frac{D}{L}\right) & \text{for } D < D_c \\ c & \text{for } D > D_c \end{cases}$. We determined that in glass tunnels of diameter above D_c = 1.03 ± 0.01 L the lateral limb span, x_{span}, was independent of tunnel size (R^2 < 0.001) with mean value of x_{span}, determined from fit parameter c = 1.04 ± 0.14 L (Fig. 2*D*). In glass tunnels of diameter less than D_c, limb posture was altered by tunnel confinement and x_{span} subsequently decreased (Fig. 2*D*). For comparison with ant-created tunnels, excavated tunnel diameter was D = 1.06 ± 0.23 L. Thus, ants modify their limb position depending on tunnel size, but maintain approximately the same rate of ascent and descent. Furthermore ants climbing within tunnels they construct are capable of using their spread-limb posture, which may have implications for locomotor stability.

The alteration of the midlimb posture in smaller tunnels suggests that a transition occurs in the direction of locomotor force production by the midlimb. In the sprawled posture, midlimb tarsi contact forces pull toward the body and the tarsal hooks and adhesive pads are likely engaged. In contrast, when the limb is in the compact posture, the limb pushes down and

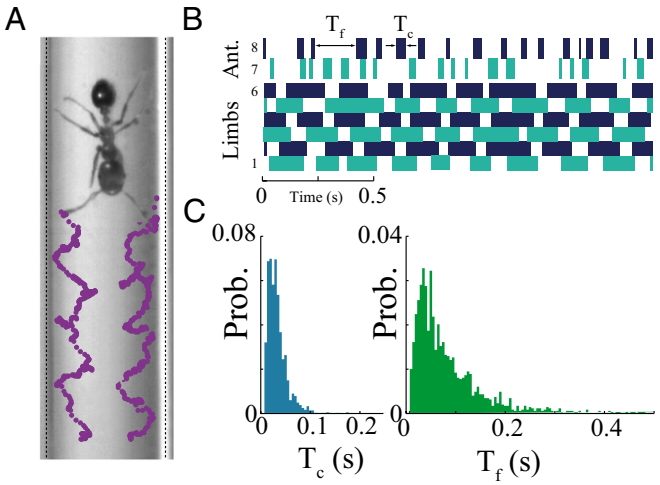

Fig. 3. Antennae use in confined locomotion. (*A*) Image of ant descending in a tunnel with tracked position of antennae tips shown in purple. D = 3 mm. (*B*) Stepping and antennae contact diagram for a vertical descent in a tunnel. Light and dark blue highlight limbs that form alternating tripods during locomotion: (1) right hind, (2) right mid, (3) right fore, (4) left fore, (5) left mid, (6) left hind. Right and left antennae are denoted by (7) and (8) respectively. Time of antennal contact, T_c, and time free, T_f, are highlighted. (*C*) Probability distribution for both T_c and T_f.

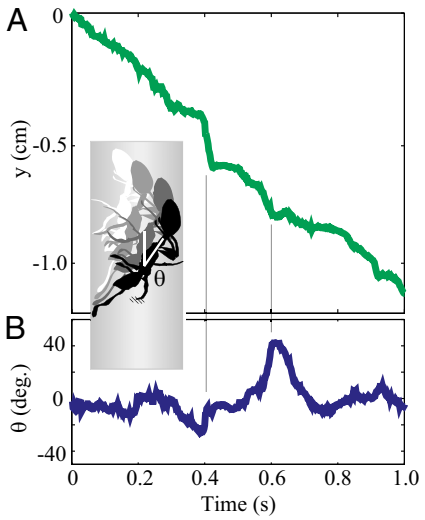

Fig. 4. Kinematics and slip recovery during tunnel climbing within an ant-constructed tunnel. (*A*) Vertical position of ant while descending (Movie S3). (*B*) Body angle (θ) with respect to tunnel axis. Two slip recovery events are highlighted by vertical gray lines. During slip events antennae and limbs are jammed against the wall and the body pitches into the tunnel wall (illustration).

away from the body to generate forward thrust. In the compact posture, to generate thrust force, we hypothesize that the rows of 50–350-μm-long spiny hairs along the limb (Fig. S8) are used in concert with limb substrate friction to engage asperities in the climbing substrate and allow the limb to push. Such multifunctional limb design has been previously shown to aid in rapid locomotion on horizontal substrates through the engagement of spiny limb hairs with rough surfaces (49).

Slip-Recovery Through Rapid Jamming. Fire ants possess a pair of elbowed antennae capable of a wide range of articulated motion about the head (Fig. 3*A*). While ascending and descending, ants rapidly placed antennae in contact with the tunnel walls (Movie S1 and Fig. 3*A*). In the glass tunnels, antennae–wall contact time was $T_c = 29 \pm 23$ ms (Fig. 3*C*; $n = 1{,}840$ contacts from 54 climbs) during head-first descent. The time between contacts was $T_f = 82 \pm 81$ ms (Fig. 3*C*). The rapid and repeated antennae–wall contact is important for tactile and chemo-sensing within the subterranean environment (34). However, observations of ants slipping within glass and natural tunnels (Movie S4) led us to hypothesize that these sensory appendages could also have important biomechanical functions for climbing in confined spaces.

During high-speed ascent and descent in both glass and ant-constructed tunnels, ants exhibited slips that were rapidly corrected through antennae and limb contact with the tunnel surface (Fig. 4 and Movies S1, S2, and S3). Ants rapidly arrested short downward slips (in which the instantaneous downward velocity exceeded 15 mm·s^{-1}) within 82 ± 21 ms ($n = 456$ slips among 54 individuals) within glass tunnels of all sizes. During head-first slips, antennae were placed against the tunnel wall before arrest in 92% of the observed slip arrests (422 antennae contacts out of 456 slips). Excluding slips in which antennae began in contact with the wall, the time between slip onset and antennae–wall contact was 32 ± 22 ms ($n = 265$).

We briefly compare our observations of tunnel falling with the more extreme case of gliding among arboreal ants, in which ants in free fall can direct their motion during falls of hundreds to thousands of body lengths (50). During aerial descent among canopy ants, gliding from a tree branch to a lower location on the tree aids in evasion from predators that may be on branches or on the forest floor. In the crowded and dark nest, long-distance–directed aerial descent would be unsuccessful due to poor navigational ability and space constraints (lack of vision and tactile sensation from antennae). However, we hypothesize that the rapid slip arrest we observe in high-speed tunnel locomotion (Movie S3 and Fig. 4) is an important mode of locomotion in confined environments, such that repeated slips or "microfalls" can enhance rapid descent.

Our observations indicate that antennae are rapidly and readily used for slip correction when climbing in confined spaces. In the case of larger slips, the antennae deformations also suggest that antennae provide significant mechanical support to the falling ant (Movie S4 and Figs. S9–S11). Morphological adaptations to subterranean life are well documented (51); here we have observed that fire ant antennae—which are evolved from ancestral arthropod limbs (52)—retain partial functionality as locomotion appendages. Antennae can act effectively like seventh and eighth limbs to arrest falls and maintain stability during climbing in tunnels.

Rapid fall arrest by bracing antennae against a tunnel wall relies on the ability to quickly jam limbs and body against opposing locations along the tunnel wall. Thus, we hypothesized that the ability to rapidly arrest slips through body jamming would be sensitive to tunnel diameter. To test this hypothesis we subjected ants climbing within glass tunnels to perturbations consisting of a rapid downward translation of the tunnels (Fig. 2*A* and Movie S5). Glass tunnels were mounted to a vertical air piston controlled through a computer. The piston translated the tunnels downward 5 mm, at which point the motion was stopped in less than 2.5 ms upon impact with the mounting plate. The final downward speed of the tunnels before impact was estimated to be 0.66 m/s; ants were thus subject to a mechanical perturbation of ∼27 g upon stopping. The perturbations used in this experiment are substantially larger than what ants experience during jostling by neighbors in the natural environment. However, high-speed perturbation-response experiments challenge the fastest neural response times of locomoting organisms, and thus help to determine the role of body kinematics and morphology in rapid locomotion stabilization (6, 10, 53, 54).

We found that 52% (1,092 falls out of 2,584 perturbations) of the perturbation experiments did not lead to ants being displaced from the tunnel wall (Fig. S12*A*). This indicates that the fire ant

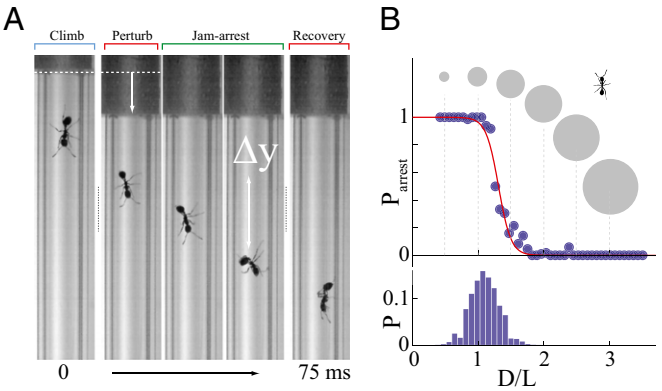

Fig. 5. Climbing perturbation experiment. (*A*) Image sequence of perturbation and recovery (corresponding to perturbation 1 in Movie S5). Left image is immediately before perturbation. Middle images show recovery that took place within 75 ms (ΔT = 30 ms for middle three frames). After perturbation recovery ant continued downward climb (right image). (*B*, *Upper*) Probability to arrest falls, P_{arrest}, versus D/L. Line is logistic fit described in text. Gray circles are tunnel diameter drawn to scale of ant illustration. (*B*, *Lower*) Probability distribution of tunnel diameter in units of ant body length (L) for excavated tunnels (data reproduced from Fig. 1*D*).

tarsi and adhesive footpads are robust to substantial perturbations, consistent with other measurements of the ant's adhesive strength (55–57). However, displacement from the tunnel surface did occur in 48% of experiments, and the outcome of perturbations was strongly influenced by the interaction of ant tunnel size.

We found that tunnel diameter, with respect to ant body length, had a significant effect on the probability to fall during a perturbation experiment, with smaller tunnels aiding in the ants' perturbation resistance (Fig. S12*B*). The probability to fall during a perturbation increased from 36% to 73% as D/L increased from 0.4 to 3.4; the increase occurred over a narrow range around D/L ≈ 2.3. The resistance to perturbation in tunnels of D < 2.3 L was likely due to the ability of fire ants to robustly engage surfaces. When climbing vertical planar surfaces, animals have to contend with gravity, which, because the animal's center of mass is offset from the climbing surface, generates an overturning moment on the animal that must be overcome. In contrast, when climbing in small tunnels, ants may be able to minimize torque-induced gravity on the body by placing limbs laterally against walls and thus keeping the center of mass in the same vertical plane as limb contact points.

Ants perturbed from the tunnel wall either arrested their fall within a vertical distance Δy, or fell to the tunnel bottom (Fig. 5*B* and Movie S5). Arrest distance, Δy, increased with increasing tunnel diameter normalized by body length, D/L (Fig. S13). The upper envelope of Δy (dashed line in Fig. S13) increased linearly with a slope 67 ± 7 mm (R^2 = 0.95). This relationship can be understood through a kinematic argument: to arrest falls, ants extend limbs and antennae toward tunnel walls that are a further distance away within larger tunnels, and this results in longer fall distances in larger tunnels (*SI Text*).

The probability to arrest a fall, P_{arrest}, within a tunnel of size D/L decreased from 1 to 0 as D/L increased. We fit P_{arrest} to a logistic function, $P_{arrest} = 1/\left[1 + e^{\frac{\alpha}{L}(D - D_s)}\right]$ (Fig. 5*B*) and found the cutoff tunnel diameter, D_s = 1.31 ± 0.02 L (α = −10.54 ± 1.76), at which arrest probability decreased to below 50% (see Fig. S5 and Table S2). Within ant-constructed tunnels (of mean diameter 1.06 L; Fig. 5*B*, *Lower*) we predict that 93% of falls will be arrested. This demonstrates that ants display a high degree of climbing stability within tunnels of comparable size to those they create (1.06 L); however, an increase in tunnel diameter by 50% reduced arrest probability to less than 5%.

We hypothesized that tunnel diameter would limit the ability to recover from falls through a "jam arrest" mechanism within tunnels. Thus, we expected that D_s was governed by morphological limitations of ant limb use. We measured the lateral limb span, x_{span}, for free-falling ants and found that ants extended limbs maximally to a width of $\max(x_{span})$ = 1.33 ± 0.22 L independent of tunnel size when D > 1.3 L. This measurement is consistent with the typical midlimb span of fire ants 1.31 ± 0.09 L reported in the literature (*SI Text* and Fig. S15) (48) and suggests ants are extending limbs maximally to re-engage the tunnel wall while falling. In tunnels whose diameter exceeded the physical reach of the ants, D > 1.3 L, ants were unable to engage walls and the arrest probability decreased substantially (Movie S5).

We return to the digging experiments—in which groups of ants constructed tunnels—to understand how ant tunnel size relates to stability in confined spaces. The average diameter of tunnels created by ants across all excavation experiments was D = 1.06 ± 0.23 L. Thus it seems reasonable to assume that fire ants construct tunnels that facilitate rapid locomotion through the enablement of slip recovery by antennae and limb jamming, without hindering limb kinematics. Many other factors are likely to influence equilibrium nest tunnel size. Traffic may be important in nest tunnel size determination as it is hypothesized that larger tunnels in the nest foraging network are due to higher traffic flow in these locations (46, 58). Further, food transportation requirements, ventilation, protection from flooding, and protection from invasion by predators or other brood raiding colonies can also influence nest structure (34). We hypothesize that the shape and size of tunnels at any time reflects the important environmental and biological factors influencing the colony at that time (37, 47). However, during incipient nest construction, such as after a flood, we expect that high-speed locomotion and excavation are important to survival.

Conclusions

We have shown that fire ants are capable of moving rapidly within their nest through the use of multifunctional limbs and antennae, which effectively engage tunnel surfaces. We found that tunnel diameter had little effect on locomotion speed over a threefold range of tunnel diameters, although body posture and limb use differed in different-sized tunnels. We also discovered that fire ant antennae were effectively used as additional limbs during locomotion. Functionality of antennae as load-bearing, locomotor appendages was a surprising result, one which highlights the importance of studying locomotion within the context of the organism's natural environment. During locomotion, antennae were rapidly and repeatedly placed in contact with the tunnel surface for sensory feedback, however the antennae's multifunctional nature also implies that antennae may be the ant's first option to rapidly recover from missteps or slips. X-ray CT indicated that fire ants constructed tunnels of appropriate size to enable utilization of the slip recovery mechanisms we observed in laboratory climbing experiments.

The ability for organisms to offload locomotion control to their environmental structures represents a new paradigm of locomotion control and a novel example of the integration of the organism's extended phenotype (the nest) for a locomotory purpose. We hypothesize that the construction of control surfaces suited to the locomotors' body size and limb kinematics reduces locomotion control requirements within subterranean environments and may be a general feature of robust control within organism-engineered substrates such as tunnels, trails, or burrows. A universal scaling of burrow cross-sectional area with body length (20)—sampled across a wide array of organisms varying by over six orders of magnitude by mass—provides evidence of the commonalities of locomotor constraints among subterranean animals. Thus, the robust locomotor control strategies for subterranean environments we have described for fire ants may apply to a diversity of subterranean animals. We also expect that our biological discoveries will provide inspiration for, and simplify control in, collective robotic devices that will have to move within confined environments such as search and rescue zones. We propose that future robot teams could enhance survival in harsh terrestrial and extraterrestrial environments through collective construction of appropriately engineered shelters and nests.

Methods

Digging Experiments. We used a custom X-ray CT system to observe tunnel excavation. Groups of 100–150 fire ant workers dug tunnels in 3.8 or 8.2 cm diameter chambers filled to a height of 12–15 cm with slightly polydisperse glass particles of diameter 50, 210, or 595 μm (Jaygo Inc.; see Table S1 for particle size distribution). We varied water moisture content in the simulated soil between 1% and 20% measured by mass. From CT reconstructions we extracted the tunnel shape using the Chan–Vese active contours method (59). We measured the effective tunnel diameter, D, as the maximum of the distance transform of the tunnel cross-section (*SI Text*).

Climbing Experiments. Climbs in ant-constructed tunnels were observed in quasi-2D arenas, 27 × 34 × 0.3 cm in size, filled with wetted granular material as described in ref. 60. Ants climbed between a nest and foraging arena through glass tunnels of diameter D 1–9 mm (in increments of 1.0 mm) and length 107.0 mm (Technical Glass). Movies of climbing ants were recorded at a frame rate of 200 and 400 Hz (AOS Technologies). To observe the falling response of ants within tunnels, we performed a perturbation experiment in

which a fixture holding the glass tunnels was mounted to a vertical, computer-controlled air piston. The air piston accelerated the tunnels from rest 5 mm downward over a time period of 0.15 s. Air piston activation was automated and triggered by ant movement, which in turn triggered the capture of high-speed video. All perturbed and unperturbed climbing experiments were performed while ants freely trafficked between the nest site and the foraging arena.

Statistics. In all experiments ant body length was measured from the base of the mandibles on the head to the tip of the gaster. Ant body length was measured by selecting points in Matlab. Statistical tests were performed in Matlab and JMP (SAS Software). Analysis of variance was used for comparisons among treatments. In digging trials we treated colony and date as random factors in an analysis of variance. For comparing the statistical significance of nonlinear regression models to data, we used the method described in Motulsky (61). All results are reported as mean ± SD.

ACKNOWLEDGMENTS. Funding support was provided by National Science Foundation Physics of Living Systems Grant 095765 and the Burroughs Wellcome Fund.

1. Lejeune TM, Willems PA, Heglund NC (1998) Mechanics and energetics of human locomotion on sand. *J Exp Biol* 201(Pt 13):2071–2080.
2. Maladen RD, Ding Y, Li C, Goldman DI (2009) Undulatory swimming in sand: Subsurface locomotion of the sandfish lizard. *Science* 325(5938):314–318.
3. Autumn K, et al. (2006) Dynamics of geckos running vertically. *J Exp Biol* 209(Pt 2): 260–272.
4. Jayaram K, et al. (2013) Running in confined spaces by the American cockroach. *Integr Comp Biol* 53(1):102.
5. Alexander RMN (2002) *Principles of Animal Locomotion* (Princeton Univ Press, Princeton, NJ).
6. Full RJ, Kubow T, Schmitt J, Holmes P, Koditschek D (2002) Quantifying dynamic stability and maneuverability in legged locomotion. *Integr Comp Biol* 42(1):149–157.
7. Dickinson MH, et al. (2000) How animals move: An integrative view. *Science* 288(5463):100–106.
8. Holmes P, Full RJ, Koditschek D, Guckenheimer J (2006) The dynamics of legged locomotion: Models, analyses, and challenges. *SIAM Rev* 48(2):207–304.
9. Goldman DI, Chen TS, Dudek DM, Full RJ (2006) Dynamics of rapid vertical climbing in cockroaches reveals a template. *J Exp Biol* 209(Pt 15):2990–3000.
10. Daley MA, Biewener AA (2006) Running over rough terrain reveals limb control for intrinsic stability. *Proc Natl Acad Sci USA* 103(42):15681–15686.
11. Li C, Umbanhowar PB, Komsuoglu H, Koditschek DE, Goldman DI (2009) From the cover: Sensitive dependence of the motion of a legged robot on granular media. *Proc Natl Acad Sci USA* 106(9):3029–3034.
12. Maladen RD, Ding Y, Umbanhowar PB, Kamor A, Goldman DI (2011) Mechanical models of sandfish locomotion reveal principles of high performance subsurface sand-swimming. *J R Soc Interface* 8(62):1332–1345.
13. Koditschek DE, Full RJ, Buehler M (2004) Mechanical aspects of legged locomotion control. *Arthropod Struct Dev* 33(3):251–272.
14. Nishikawa K, et al. (2007) Neuromechanics: An integrative approach for understanding motor control. *Integr Comp Biol* 47(1):16–54.
15. Loeb G (1995) Control implications of musculoskeletal mechanics. *Ann Int Conf IEEE-EMBS* 17:1393–1394.
16. Kaspari M, Weiser M (2007) The size–grain hypothesis: Do macroarthropods see a fractal world? *Ecol Entomol* 32(3):279–282.
17. Kaspari M, Weiser M (1999) The size–grain hypothesis and interspecific scaling in ants. *Funct Ecol* 13(4):530–538.
18. Reichman O, Smith SC (1990) Burrows and burrowing behavior by mammals. *Current Mammalogy* 2:197–244.
19. Nevo E (1979) Adaptive convergence and divergence of subterranean mammals. *Annu Rev Ecol Syst* 10:269–308.
20. White CR (2005) The allometry of burrow geometry. *J Zool (Lond)* 265(04):395–403.
21. Tschinkel WR (2003) Subterranean ant nests: Trace fossils past and future? *Palaeogeogr Palaeoclimatol Palaeoecol* 192(1):321–333.
22. White C (2001) The energetics of burrow excavation by the inland robust scorpion, Urodacus yaschenkoi (Birula, 1903). *Aust J Zool* 49(6):663–674.
23. Lovegrove B (1989) The cost of burrowing by the social mole rats (Bathyergidae) Cryptomys damarensis and Heterocephalus glaber: The role of soil moisture. *Physiol Zool* 62(2):449–469.
24. Vleck D (1979) The energy cost of burrowing by the pocket gopher Thomomys bottae. *Physiol Zool* 52(2):122–136.
25. Ebensperger LA, Bozinovic F (2000) Energetics and burrowing behaviour in the semifossorial degu Octodon degus (Rodentia: Octodontidae). *J Zool (Lond)* 252(2): 179–186.
26. Sluyter F, Bult A, Lynch CB, van Oortmerssen GA, Koolhaas JM (1995) A comparison between house mouse lines selected for attack latency or nest-building: Evidence for a genetic basis of alternative behavioral strategies. *Behav Genet* 25(3):247–252.
27. Weber JN, Peterson BK, Hoekstra HE (2013) Discrete genetic modules are responsible for complex burrow evolution in Peromyscus mice. *Nature* 493(7432):402–405.
28. Dawkins R (1999) *The Extended Phenotype: The Long Reach of the Gene* (Oxford Univ Press, New York).
29. Horner AM, Biknevicius AR (2010) A comparison of epigean and subterranean locomotion in the domestic ferret (Mustela putorius furo: Mustelidae: Carnivora). *Zoology (Jena)* 113(3):189–197.
30. Wilson EO (1976) The organization of colony defense in the ant Pheidole dentata Mayr (Hymenoptera: Formicidae). *Behav Ecol Sociobiol* 1(1):63–81.
31. Wilson EO (1986) The organization of flood evacuation in the ant genus pheidole (Hymenoptera, Formicidae). *Insectes Soc* 33(4):458–469.
32. Kimchi T, Terkel J (2004) Comparison of the role of somatosensory stimuli in maze learning in a blind subterranean rodent and a sighted surface-dwelling rodent. *Behav Brain Res* 153(2):389–395.
33. Dussutour A, Fourcassié V, Helbing D, Deneubourg JL (2004) Optimal traffic organization in ants under crowded conditions. *Nature* 428(6978):70–73.
34. Hölldobler B, Wilson EO (1990) *The Ants* (Belknap, Cambridge, MA).
35. Traniello JFA (1989) Foraging strategies of ants. *Annu Rev Entomol* 34(1):191–210.
36. Oster GF, Wilson EO (1979) *Caste and Ecology in the Social Insects (MPB-12)* (Princeton Univ Press, Princeton).
37. Tschinkel W (2006) *The Fire Ants* (Belknap, Cambridge, MA).
38. Hölldobler B (1999) Multimodal signals in ant communication. *J Comp Physiol A Neuroethol Sens Neural Behav Physiol* 184(2):129–141.
39. Julian GE, Gronenberg W (2002) Reduction of brain volume correlates with behavioral changes in queen ants. *Brain Behav Evol* 60(3):152–164.
40. Markl H (1965) Stridulation in leaf-cutting ants. *Science* 149(3690):1392–1393.
41. Spangler HG (1967) Ant stridulations and their synchronization with abdominal movement. *Science* 155(3770):1687–1689.
42. Hill PSM (2001) Vibration and animal communication: A review. *Am Zool* 41(5): 1135–1142.
43. Wilson EO (1962) Chemical communication among workers of the fire ant *Solenopsis saevissima* (Fr. Smith) 1. The organization of mass-foraging. *Anim Behav* 10(1): 134–147.
44. Jackson BD, Morgan ED (1993) Insect chemical communication: Pheromones and exocrine glands of ants. *Chemoecology* 4(3):125–144.
45. Markin GP (1974) Foraging tunnels of the red imported fire ant, *Solenopsis invicta*. *J Kans Entomol Soc* 48(1):84.
46. Cassill D, Tschinkel W (2002) Nest complexity, group size and brood rearing in the fire ant, Solenopsis invicta. *Insectes Soc* 49(2):158–163.
47. Markin GP, Dillier JH, Collins H (1973) Growth and development of colonies of the red imported fire ant, Solenopsis invicta. *Ann Entomol Soc Am* 66(4):803–808.
48. Tschinkel WR, Mikheyev AS, Storz SR (2003) Allometry of workers of the fire ant, Solenopsis invicta. *J Insect Sci* 3(2):1–11.
49. Spagna JC, Goldman DI, Lin PC, Koditschek DE, Full RJ (2007) Distributed mechanical feedback in arthropods and robots simplifies control of rapid running on challenging terrain. *Bioinspir Biomim* 2(1):9–18.
50. Yanoviak SP, Dudley R, Kaspari M (2005) Directed aerial descent in canopy ants. *Nature* 433(7026):624–626.
51. Nevo E (1999) *Mosaic evolution of subterranean mammals: regression, progression, and global convergence* (Oxford Univ Press, New York).
52. Grimaldi D, Engel MS (2005) *Evolution of the Insects* (Cambridge Univ Press, New York).
53. Jusufi A, Goldman DI, Revzen S, Full RJ (2008) Active tails enhance arboreal acrobatics in geckos. *Proc Natl Acad Sci USA* 105(11):4215–4219.
54. Ristroph L, et al. (2010) Discovering the flight autostabilizer of fruit flies by inducing aerial stumbles. *Proc Natl Acad Sci USA* 107(11):4820–4824.
55. Federle W, Baumgartner W, Hölldobler B (2004) Biomechanics of ant adhesive pads: Frictional forces are rate- and temperature-dependent. *J Exp Biol* 207(Pt 1):67–74.
56. Federle W, Brainerd EL, McMahon TA, Hölldobler B (2001) Biomechanics of the movable pretarsal adhesive organ in ants and bees. *Proc Natl Acad Sci USA* 98(11): 6215–6220.
57. Endlein T, Federle W (2013) Rapid preflexes in smooth adhesive pads of insects prevent sudden detachment. *Proc R Soc B* 280(1757):20122868.
58. Tschinkel WR (2011) The organization of foraging in the fire ant, Solenopsis invicta. *J Insect Sci* 11(26). Available at insectscience.org/11.26.
59. Chan T, Vese L (2001) Active contours without edges. IEEE Transactions on Image Processing 10(2):266–277.
60. Gravish N, et al. (2012) Effects of worker size on the dynamics of fire ant tunnel construction. *J R Soc Interface* 9(77):3312–3322.
61. Motulsky HJ, Ransnas LA (1987) Fitting curves to data using nonlinear regression: A practical and nonmathematical review. *FASEB J* 1(5):365–374.

Supporting Information

Gravish et al. 10.1073/pnas.1302428110

SI Text

SI Methods

Ant Collection and Care. The *Solenopsis invicta* colonies were collected during the spring of 2012 from roadsides outside of Atlanta, GA. Nests were excavated and transported to the laboratory and ants were separated from the soil using the water drip method (1). Colonies were housed in open plastic bins in a temperature-controlled room with 12 h on, 12 h off lighting. Colonies were provided ad libitum water and insect larvae as food.

Digging Experiments. The digging arenas were placed on a rotating stage controlled by a stepper motor (Lin Engineering), which was located 76 cm from a 110 kVp, 3 mA X-ray source. An image intensifier was located 103 cm from the source and a Phantom v210 camera (Vision Research) was used to visualize the X-ray images. Samples images were taken at angular increments of 0.9°. We chose tunnels that were not adjacent to a wall (Fig. S1) and extracted the tunnel shape using the Chan–Vese active contours method (2). Tunnel properties were measured using the Matlab image morphology toolbox. We computed the distance transform of the tunnel shape using the Matlab command *bwdist* and considered the maximum value of the distance transform as the effective tunnel diameter.

Digging experiment 1. Groups of fire ant workers were challenged to dig tunnels in the laboratory. The 8.2 cm diameter cylindrical containers were filled to a depth of 12 cm with a dry granular material of particle size 250 ± 50 μm (Jaygo Inc., Dragonite Soda Lime Glass beads, #5210). Arenas were first fully immersed in water to saturate the soil and then allowed to drain for 1 h. Wet soil is known to induce digging in natural fire ant nests (3). Workers were introduced into the arena and were allowed to dig for 24 h with a constant light source maintained above to stimulate digging. We evaluated the tunnel cross-section shape at various depths among 10 separate digging trials, each containing multiple tunnels, which resulted in 2,262 observations of tunnel diameter.

Digging experiment 2. In a second set of nest construction experiments, we varied soil moisture content and particle size. We used collections of glass beads of diameter 50, 210, or 595 μm (See Table S1 for polydispersity), which were mixed with water and prepared at moisture contents of 1%, 3%, 5%, 10%, 15%, and 20% (measured by mass). Table S1 summarizes particle size distribution. Digging substrate was placed in a 3.8-cm-diameter cylindrical digging arena filled to a height of 14.5 cm. A 1 cm diameter plastic tube inserted into the center of the surface constrained the workers to initiate digging away from walls. We generated uniform compaction of the moistened media by sieving the wetted granular material through a mesh grid with 1 mm grid spacing using VTS 500 single vibrator system. Groups of 100 workers were introduced into the digging arenas, and we evaluated tunnel shape in CT scans at 10, 15, and 20 h. Eight separate colonies were tested at each particle size and moisture content combination resulting in 185 excavation experiments. We measured tunnel depth and cross-sectional shape at a depth of half the tunnel depth. We tested for the effect of particle size, water content, and the interaction (particle size)×(water content) using an analysis of variance in which colony and test date were treated as random effects.

Climbing Experiments. ***Arena experiments.*** Quasi-2D arenas, 27 × 34 × 0.3 cm^3 in size, were filled with the same wetted granular material as described in *Digging experiment 1* (above) and were prepared to allow for ant visualization during locomotion (see ref. 4 for details). A group of 150 ants excavated in the simulated soil for 48 h. We observed tunnel locomotion using a macro-lens and a Phantom v210 camera, capturing video at 500 Hz. We encouraged high-speed ascent and descent through ant-created tunnels by triggering an alarm response among the workers in which we exhaled gently into the nest entrance at the top surface.

Glass tunnel climbing experiments. We used a simulated nest environment to study ant climbing in smooth glass tunnels in which we could view the interaction of all limbs and antennae with the climbing substrate (Fig. 2). An enclosed, light-proof box that contained a wetted porous floor (plaster of paris) served as a nest, and housed 150–300 worker ants during the course of an experiment. The simulated nest was connected to a foraging arena through a series of nine glass vertical observation tunnels ranging in inner diameter from 1–9 mm in increments of 1 mm. Tunnels were 107 mm long, and we observed a 96 mm length of them. Tunnels were illuminated by LED lights for visualization with a high-speed camera. Ad libitum water and food were provided in the foraging arena, which encouraged worker traffic to and from the nest. A heat lamp was placed over the foraging arena to create a temperature gradient between the "above-surface" foraging arena and the "subterranean" simulated nest. The simulated nest and foraging arena setup encouraged ants to freely traffic within the tunnels and allowed us to observe tunnel climbing while performing a natural, unperturbed behavior.

Ant climbing posture was computed in Matlab in which we isolated the ant body from the stationary background using an active contours algorithm (2). We computed the vertically oriented bounding box of the ant profile with the horizontal dimension of this box representing x_{span}. Climbing ants could be found at any angular location along the tunnel wall, and thus we removed all runs in which ants were visualized from the lateral sides. Furthermore, in measuring horizontal limb span we only included ant postures in which the body axis measured from gaster to head deviated from the vertical by less than 10°. This resulted in 483,525 observations of climbing posture from all phases within the stride.

Glass tunnel perturbation experiments. To observe the falling response of ants within tunnels we performed a perturbation experiment. Glass tunnels were mounted to a vertical air piston maintained at 551 kPa and controlled through a computer. The piston's motion stopped upon impact with the mounting plate, and vertical motion halted in less than 2.5 ms. We calculated that the final downward speed of the tunnels before impact was 0.66 m/s, which suggests that ants were subject to a mechanical perturbation of ∼27 g upon stopping.

Activation of the air piston was controlled by a computer program that monitored motion in the upper portion of the tunnel region. When an ant was detected entering this region, a relay was activated that controlled a high-speed solenoid that engaged the air piston. Simultaneously a trigger signal was sent to a high-speed camera (AOS Technologies) that captured 2-s perturbation response videos at 1024 × 1280, 400 frames per second and 500 μs exposure time. Analysis of perturbation experiments was performed using Matlab image analysis tools. Users determined fall distance, ant length, ant orientation, fall time, and fall code (successful arrest, no arrest, no fall) from the perturbation response videos. We observed 2,268 perturbation response experiments among worker ants from five of the six host colonies (B–F).

SI Discussion

X-Ray Computed Tomography Results Data Analysis. We performed digging trials in 3D cylindrical containers of outer diameter 3.8 cm and 8.2 cm. We identified tunnels that were not adjacent to the container wall, and we extracted out their shape using an active contours algorithm as described in *Methods* (Fig. S1). We characterized tunnel shape using two methods: (*i*) fitting an ellipse to the tunnel cross-section at different depths and (*ii*) computing the distance transform of tunnel image mask, and multiplying the maximum by a factor of two. The distance transform of the image measures the nearest Euclidean distance to a tunnel wall at every pixel location within the tunnel mask. Taking the maximum value of the distance transform for a given tunnel cross-section in effect estimates the "worst-case scenario" location for an ant to fall in that tunnel because that location is furthest away from tunnel surfaces. Since we are focused on locomotion stability, we use the maximum of the distance transform as the metric for local tunnel size and further refer to this as tunnel diameter in the text.

Tunnels were primarily circular (Fig. S1) with major diameter $D_{maj} = 4.2 \pm 1.0$ mm and minor diameter $D_{maj} = 3.5 \pm 0.9$ mm, however there were significant cases in which tunnel shape deviated from a simple ellipse (Fig. S2), which warranted use of the distance transform technique. We note that since tunnels were primarily circular in cross-section (see ratio of major and minor axes in Fig. S2*E*) the difference between tunnel size measured by ellipse fit or distance transform was small. Comparing the ellipse fit and image transform metric, we find that the measured tunnel size in both cases have median values near unity (in units of ant body length, 1.04 L for image transform, and 1.15 L for ellipse). The distributions only differ substantially in the cases of larger tunnel diameters as expected from the case study in Fig. S2. Thus, all references to diameter of ant-constructed tunnels are determined using the image distance method.

We evaluated tunnel diameter and maximum depth from CT data after 10 and 20 h of digging. Tunnel diameter did not increase over time [one-sample t test of relative change in diameter $\frac{D_{20h} - D_{10h}}{D_{10h}}$; $t(34) = 0.7467$, $P = 0.4604$] and instead incipient nests were enlarged through tunnel lengthening [one-sample t test of relative change in length $\frac{l_{20h} - l_{10h}}{l_{10h}}$; $t(49) = 5.3644$, $P < 0.0001$] consistent with a previous study of fire ant nest construction (4). We measured tunnel excavation in a diversity of idealized soil substrates of varied moisture content and particle size (Fig. S3). We found that both particle size and soil moisture had a significant effect on the maximum depth of tunnels over 20 h. However, we found no significant effect on soil moisture content or particle size on tunnel diameter. Thus, the differences observed in tunnel depth indicate that soil substrate properties did influence the digging ability of tunnel construction workers. However, the lack of significant change in tunnel cross-sectional morphology as a function of these varied simulated soil conditions suggests that tunnel shape is actively controlled for by the tunnel construction workers.

Colony-Level Demographics from Glass Tunnel Experiments. We used ant groups drawn from six host colonies (A–F) for locomotion studies and five host colonies for perturbation experiments (B–F). We measured the body length of ants ascending and descending within tunnels and find that body length significantly differed among the host colonies (Fig. S4*A*; $F_{5,2605} = 45.89$, $P < 0.0001$). We do not expect that the small differences (less than 15% difference between largest and smallest ant length among colonies) among workers influenced any of the biomechanics results we present in this study. Furthermore all results were normalized by ant length to reduce possible variance due to differences in worker size. Worker size distribution within a fire ant colony varies as the colony ages, with older colonies having larger workers (3). Thus, the differences in worker size likely reflect the variance in host colony age.

We also observed significant differences in climbing speeds among the different colonies (Fig. S4*B*). Host colony had a significant effect on ascending climbing speed ($F_{5,1615} = 33.2$, $P < 0.0001$). The difference in speed between the fastest and slowest mean speeds among colonies was 28%. We also observed a significant effect of colony on descending climbing speeds (Fig. S4*C*; $F_{5,984} = 6.06$, $P < 0.0001$), however the difference between the fastest and slowest mean speeds observed was only 12% in the case of descending. The difference in speed may indicate different propensities to forage or explore among the colonies (observed tunnel locomotion consisted of workers moving between nest and foraging arena).

We observed small differences in the stability onset in P_{arrest}, measured in perturbation experiments. All colonies exhibited a transition from 100% arrest probability in small tunnels (D/L slightly larger than unity) and 0% arrest probability in large tunnels (D/L greater than 3). We characterize the stability onset as the parameter μ from the logistic fit function of arrest probability $p_{arrest} = 1/[1 + e^{\frac{\sigma}{L}(D-\mu)}]$. We find that μ varied with colony fit value and 95% confidence intervals given in Table S2. As seen in Fig. S5, all colonies exhibited a stability transition between 1.21 and 1.56 D/L evaluated over a range of D/L = 0.41–5.17.

Comparison of Locomotion Kinematics in Glass and Ant-Created Tunnels. The ascending and descending speed–frequency relationships in both ant-constructed and glass tunnels were similar (Fig. S6). In all cases speed increased with increasing stride frequency and this relationship was well described by a quadratic equation. We quantitatively compare the speed–frequency relationship between ant-constructed and glass tunnels to determine if ants modulate their gross climbing kinematics as a function of substrate. We fit functions of the form $v = ax^2 + bx$ to the speed–frequency kinematic relationship. To test for significant differences in climbing kinematics among ant-constructed tunnels and glass tunnels, we use the method described in ref. 4, in which we compare the degrees of freedom and sums of squares of the individual fits and the data pooled together using an F test. In the case of ascending climbs, comparison between glass (D = 3–4 mm) and natural tunnels, we find no significant difference between the fit parameters from individually fit ant-constructed and glass tunnel data versus the pooled data ($F_{2,361} = 1.8150$, $P = 0.1643$). Ascending climbs were best fit with parameters $a = 0.041 \pm 0.01$ L s and $b = 0.405 \pm 0.15$ L ($R^2 = 0.95$). We find a statistically significant difference in speed–frequency relationship between glass ($a = 0.022 \pm 0.01$ L s and $b = 0.472 \pm 0.045$ L, $R^2 = 0.80$) and ant-constructed tunnels ($a = -0.011 \pm 0.013$ L s and $b = 0.911 \pm 0.140$ L, $R^2 = 0.91$) in the case of descending. Individual fits of the glass tunnel and ant-constructed tunnels statistically describe the data better than when pooled ($F_{2,252} = 113.9$, $P < 0.001$). We note that the difference between ant-constructed tunnels and glass tunnels may be because ants move in a different locomotor mode (possibly through frequent slips) when descending at such high speeds as in ant-constructed tunnels.

Midlimb Morphology and Posture Statistics. To quantify differences between the confined and unconfined locomotor postures we measured the fore–aft component of the anterior extreme position (AEP), the distance from petiole (the thin, central segment of the ant body) to limb touchdown, for the fore-limb, midlimb, and rear limb (Fig. S8). We isolated runs from two separate tunnel size treatments (small, $0.6 < D/L < 0.75$, $n = 12$; large, $2 < D/L < 2.25$, $n = 15$) that were at similar velocity (2.5 ± 0.18 L/s) and measured limb touchdown locations. We observed a significant change in AEP for all three limbs (Fig. S8). Forelimb touchdown distance significantly increased from 0.74 ± 0.04 L in the large treatment to 0.82 ± 0.02 L in the small treatment

(t_{25} = –5.7862, $P < 0.001$). Midlimb distance significantly decreased from 0.46 ± 0.04 L in the large treatment to 0.12 ± 0.04 L in the small treatment (t_{25} = 22.55, $P < 0.001$). Rear limb distance decreased from –0.53 ± 0.04 L in the large treatment to –0.32 ± 0.03 L in the small treatment (t_{25} = –13.0435, $P < 0.001$). Thus, all three limb pairs underwent a transition in kinematics between conditions of large tunnels, which allow for full limb mobility, to small tunnels, which constrain limb motion and require a postural alteration.

Evidence of Antennae Use During Falling. We observed that in perturbed and unperturbed falls, ants placed antennae against the tunnel wall and deflected or halted their center of mass motion about these antennae–tunnel contact points. Fig. S9 shows an unperturbed fall in which the antennae are spread toward the wall at the initiation of a fall. In this example, the ant fell a distance of approximately two body lengths and arrested the fall through a combination of antennae and limb contact with the tunnel wall. Following this fall, the ant continued descending within the tunnel and the tracked points after the fall show the use of antennae while climbing down. In Figs. S10 and S11, we show eight additional examples of antennae use during unperturbed head-first falls. Video of each fall is shown in Movie S4.

Perturbation Experiment Statistics. We found that in 52% (1,092 falls out of 2,584 perturbations) of the perturbation experiments, ants were not displaced from the tunnel wall (Fig. S12*A*). Tunnel diameter, with respect to ant body length, had a significant effect on the probability to fall during a perturbation experiment, with smaller tunnels aiding in the ants' perturbation resistance (Fig. S12*B*). We fit the fall probability with a logistic function $p_{fall} = a + \left[b / \left[1 + e^{\frac{g}{L}(D_f - D)}\right]\right]$ (a = 0.37 ± 0.05, b = 0.36 ± 0.09, α = 12.69 ± 17.95, D_f = 2.3 ± 0.2). The probability to fall during a perturbation doubled from 36% when D < 2.3 L to 73% when D > 2.3 L.

We measured the distance perturbed ants fell, Δy, within tunnels of different diameter (Fig. S13). We found that fall distance increased with increasing tunnel diameter. To gain insight into this relationship, we construct a simple model of fall arrest in tunnels. We assume that falling ants must extend their limbs to regain contact with the wall. We define the lateral limb distance from the body axis as l, and the distance the limb is from the wall as $\Delta l = D - l$ (we assume the ant is in the center of the tunnel). An ant falling from rest under gravity will accelerate downward with a vertical position as a function of time given by $\Delta y = \frac{1}{2} g t^2$. We assume that the limbs are accelerated outwards from the body at a constant rate, a, which results in horizontal limb position $l = \frac{1}{2} a t^2$. Eliminating t^2 from the two equations we obtain the relation $\Delta y = \frac{g}{a} l$, which can be put in terms of tunnel diameter as $\Delta y = \frac{g}{a}(D - \Delta l)$. Thus, we see that fall distance scales linearly with tunnel diameter and the upper envelope of arrest points is well approximated by a line.

Falling Posture and Lateral Limb Span. For each perturbation experiment, we measured the lateral distance, x_{span}, that falling ants extended limbs and antennae to in the horizontal plane as a function of time (Fig. S14). Ants perturbed from tunnel walls extend their limbs and antennae laterally away from their body to re-engage contact with the tunnel surface during a fall. To determine the maximum lateral limb and antennae span ants display when falling, we measured the maximum of x_{span}. We find that max(x_{span}) was limited by tunnel diameter in tunnels D < 1.3 L and was fit by a linear equation, max(x_{span}) = aL (a = 1.18 ± 0.13, R^2 = 0.71). In tunnels of D > 1.3 L, max(x_{span}) was independent of tunnel size (R^2 = 0.05) with value max(x_{span}) = 1.33 ± 0.22 L. These measurements indicate the limits of limb–antennae extension when attempting to arrest falls. The value of maximum limb extension equal to 1.33 L suggests that in tunnels above 1.33 L in diameter, we should not observe jamming mode arrest and successful arrest of falls should decrease. This is supported by the logistic fit parameters of P_{arrest} in which the transition from successful arrest to unsuccessful arrest occurs at a critical tunnel size of 1.31 ± 0.2 L.

Morphological Measurements of Fire Ants to Estimate Stability Limits for Tunnel Arrest. Using data from ref. 5, we estimated the maximum limb and antennae span fire ants were able to reach while falling (Fig. S15). We estimate the antennae span (d_1 = 0.86 ± 0.08 L) as two times the total antennal length (scape length + club length). We estimate midlimb span, denoted simply as limb span (d_2 = 1.31 ± 0.09 L), as two times the total leg length (femur + tibia + tarsi) of the midlimb. Lastly we estimate the full length along the head–gaster body axis (d_3 = 1.85 ± 0.09 L) as the antennae length + head length + alitonum length + hind limb length.

1. Gravish N, et al. (2012) Effects of worker size on the dynamics of fire ant tunnel construction. *J R Soc Interface* 9(77):3312–3322.
2. Chan T, Vese L (2001) Active contours without edges. *IEEE Transactions on Image Processing* 10(2):266–277.
3. Tschinkel W (2006) *The Fire Ants* (Belknap, Cambridge, MA).
4. Ristroph L, et al. (2010) Discovering the flight autostabilizer of fruit flies by inducing aerial stumbles. *Proc Natl Acad Sci USA* 107(11):4820–4824.
5. Tschinkel WR (2011) The organization of foraging in the fire ant, Solenopsis invicta. *J Insect Sci* 11(26):11.

Fig. S1. Overview of the X-ray CT digging trials. (*A*) Digging arena consisted of a circular plastic, or aluminum container of diameters 8.2 or 3.8 cm, filled to a height of ~12–15 cm with a simulated soil of monodisperse 50, 210, or 595 μm diameter, wetted, glass beads. 8.2 cm diameter container shown in *left* and *right* images of (*A*). (*B*) A horizontal cross-section from X-ray CT reconstruction at a depth of 6.8 cm from the surface. Top and bottom arrow indicate two tunnels not adjacent to arena wall. Four other tunnels are present but against the tunnel wall. (*C*) Cross-section of the top (*Left*) and bottom (*Right*) tunnels from *B* with extracted tunnel shape from active contours method shown as green (*Left*) and purple (*Right*) lines.

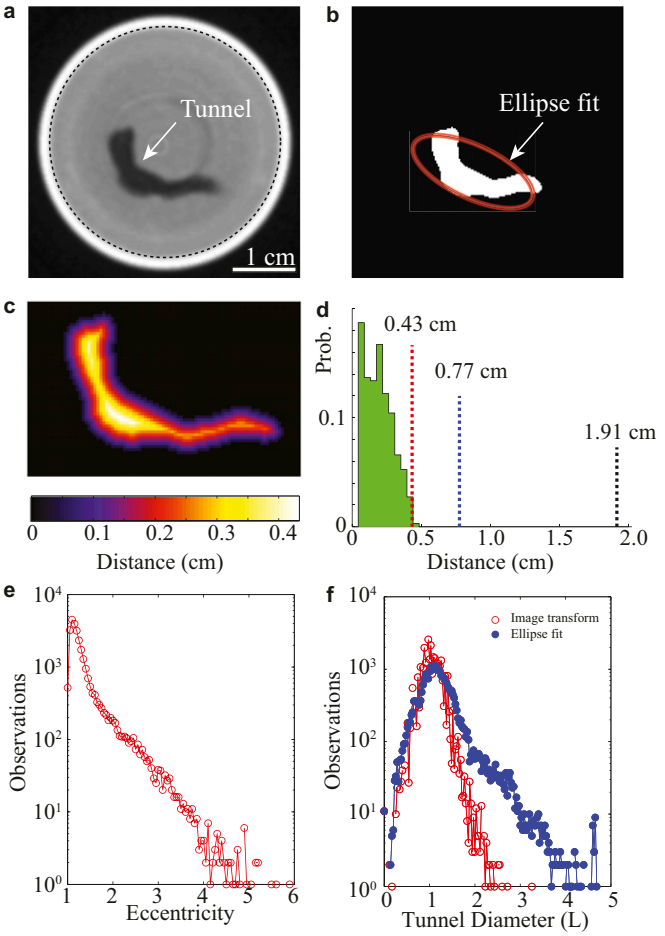

Fig. S2. Tunnel morphology analysis from X-ray CT data. (*A*) Tunneling experiment in a 3.8 cm outer diameter tube. Inner wall of digging arena shown as dashed line. An oblong-shaped tunnel is highlighted in the center of the arena. (*B*) Elliptical fit of tunnel shape. (*C*) Euclidean distance image metric of tunnel shape. Color represents minimum distance of each pixel location to tunnel wall. (*D*) Comparison of ellipse and image distance transform measures. Histogram of distance metric evaluated at all points in tunnel mask (green). Vertical dashed black line is major axis length from elliptical fit, dashed blue line is minor axis, and red line is maximum distance measured from distance transform. (*E*) Distribution of eccentricity defined as major axis divided by minor axis from fitted ellipse fits. (*F*) Distribution of tunnel diameter measured from distance transform and ellipse fit.

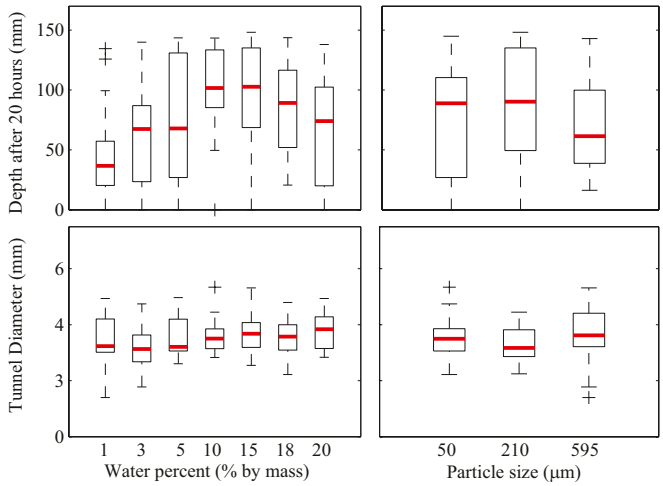

Fig. S3. Tunnel morphology as a function of particle size (left column) and water percent (right column). Box plots of maximum tunnel depth after 20 h are plotted along the top row, and box plots of tunnel diameter are plotted along the bottom row. We find that particle diameter and water percent statistically affected tunnel depth, but did not statistically affect tunnel diameter.

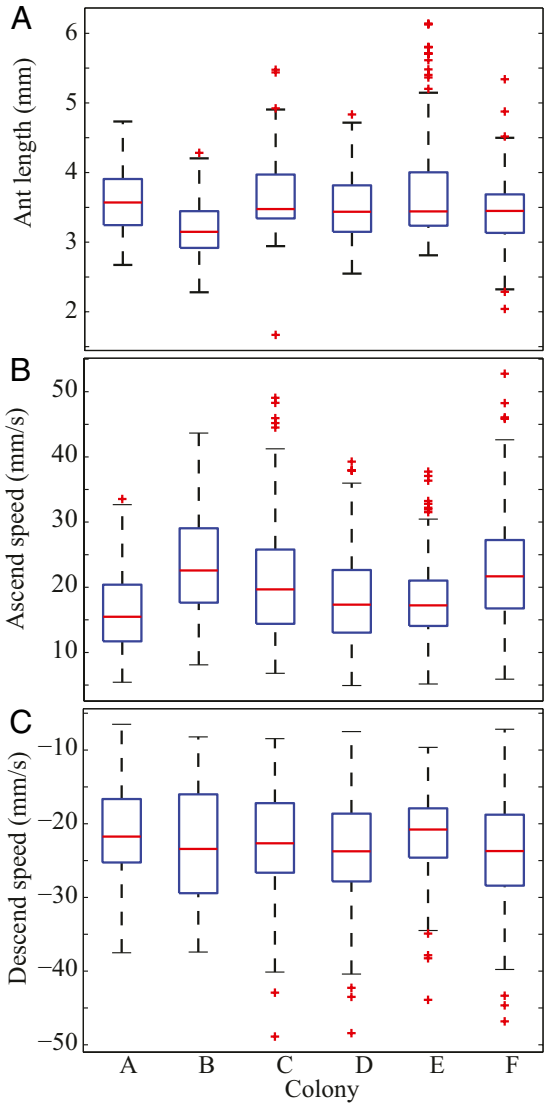

Fig. S4. Colony-level demographics and speeds for the six colonies used in experiments. Red line is median value, blue box indicates 25% and 75% quartiles, and black dashed lines highlight maxima and minima. Red squares are outliers. (*A*) Ant size distribution of different colonies. (*B*) Descending speed of different colonies. (*C*) Ascending speed of different colonies.

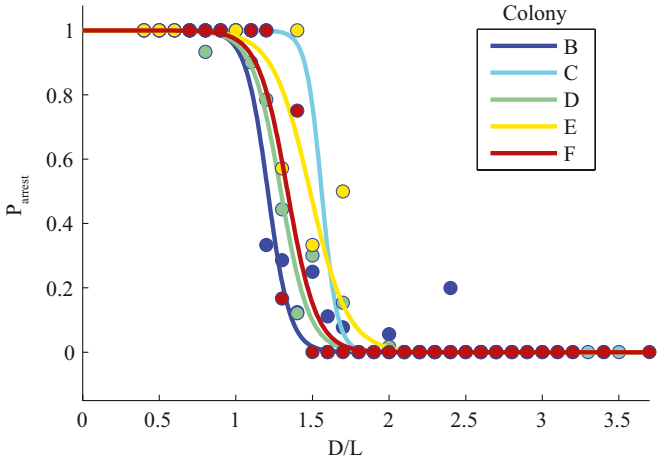

Fig. S5. P_{arrest} with logistic fit for all colonies. Colonies denoted by symbol and line color as shown in legend.

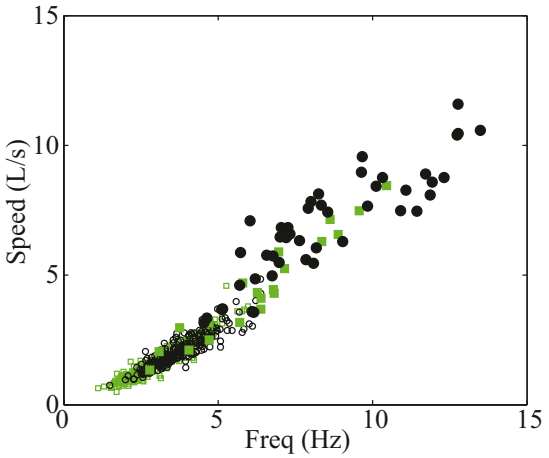

Fig. S6. Climbing speed–frequency relationship in glass tunnels of diameter 3 and 4 mm (open symbols) and ant-constructed tunnels (closed symbols). Ascending climbs are shown as open and closed green squares. Descending climbs are open and closed circles.

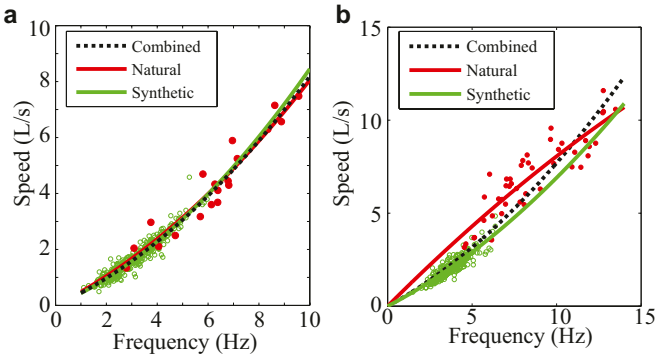

Fig. S7. Climbing speed–frequency relationship in glass tunnels of diameter 3 and 4 mm (open symbols) and ant-constructed tunnels (closed symbols). (*A*) Ascending speed–frequency relationship in ant-constructed and glass tunnels. Fit functions from natural, glass, and pooled data sets shown. (*B*) Descending speed–frequency relationship in ant-constructed and glass tunnels. Fit functions from ant-constructed tunnels, glass tunnels, and pooled data sets (combined) shown.

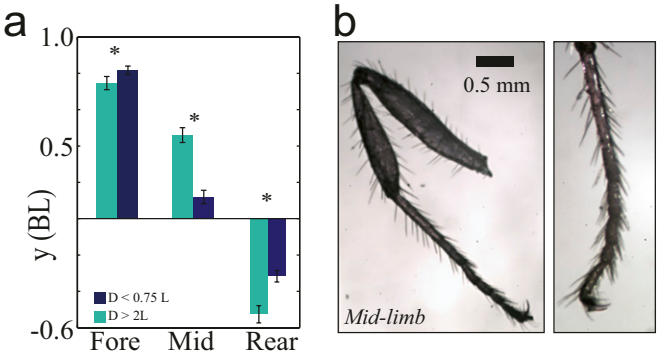

Fig. S8. Posture changes in two different sizes of tunnel. (*A*) Fore-, mid-, and hind limb touchdown distances in small (D < 1 L) and large (D > 2 L) tunnels. (*B*) Visible light microscope images of *S. invicta* worker midlimb showing the hairs that line the limb pointing distally.

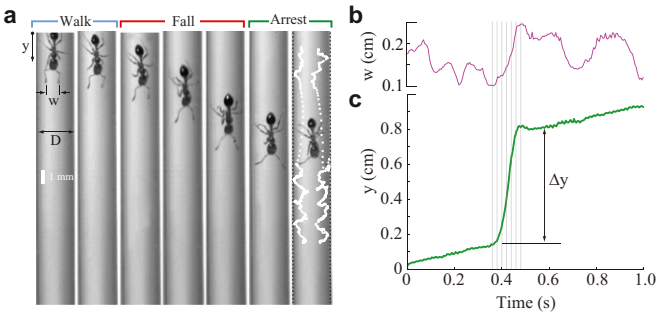

Fig. S9. Fall and arrest using antennae. (*A*) Time-lapse images of an ant descending in a tunnel. Images are separated by 10 ms. White dots in last frame show tracked position of antennae before, during, and after fall. (*B* and *C*) Instantaneous antennae width (*Upper*) and vertical position of ant body (*Lower*) during the fall arrest. Gray lines indicate images in *A*. Δy indicates fall distance.

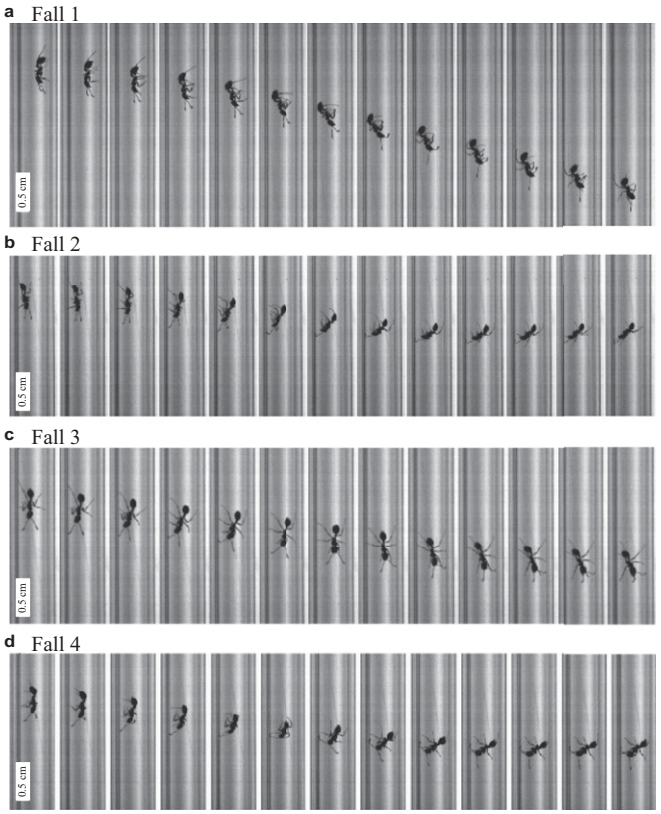

Fig. S10. Four unperturbed, head-first, fall arrest sequences in glass tunnels. All falls illustrate use of antennae during fall arrest. Images are separated by 5 ms time intervals. (*A–D*) All falls in tunnel size D = 4 mm.

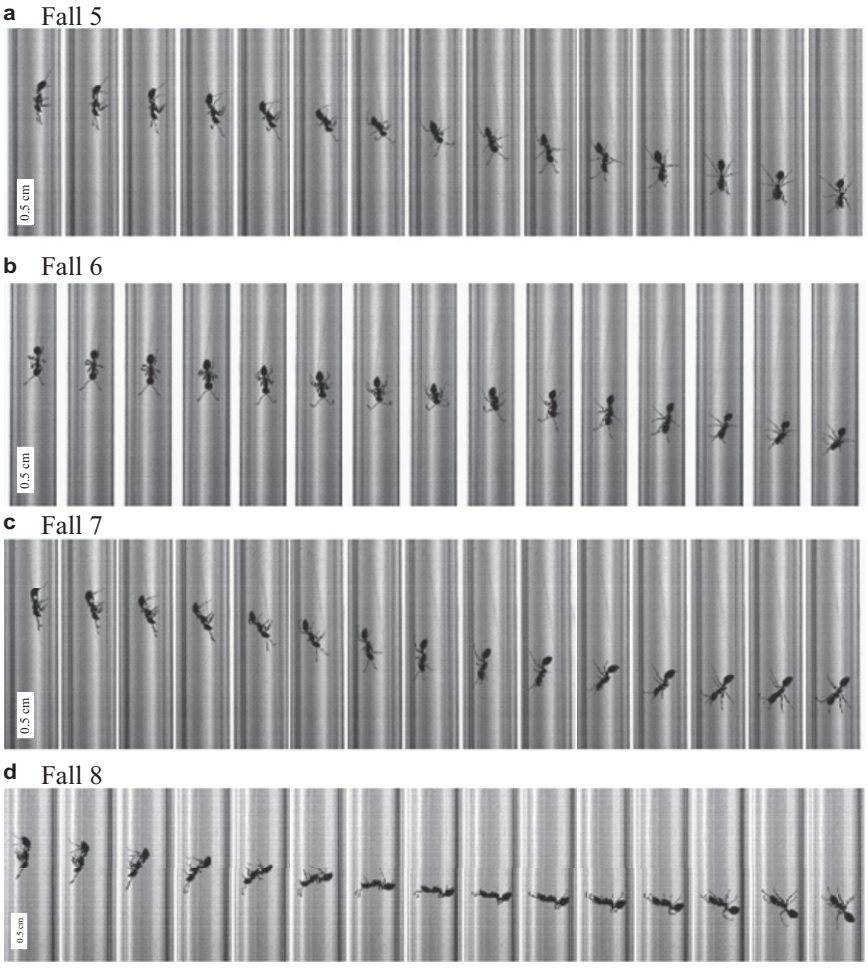

Fig. S11. Four unperturbed, head-first, fall arrest sequences in glass tunnels. All falls illustrate use of antennae during fall arrest. Images are separated by 5 ms time intervals. Tunnel size D = 4 mm (*A*), 4 mm (*B*), 4 mm (*C*), and 6 mm (*D*).

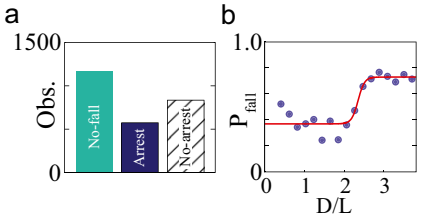

Fig. S12. Falling statistics. (*A*) Number of observations from perturbation experiments. (*B*) Probability to fall during a perturbation experiment as a function of D/L. Red line is logistic fit described in text.

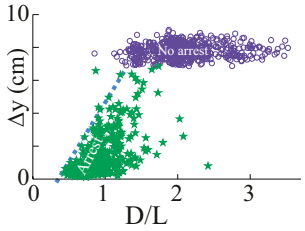

Fig. S13. Correlation between tunnel morphology D/L and fall distance. Fall distance, Δy, as a function of D/L. Purple circles indicate no arrest, while green stars indicate arrest.

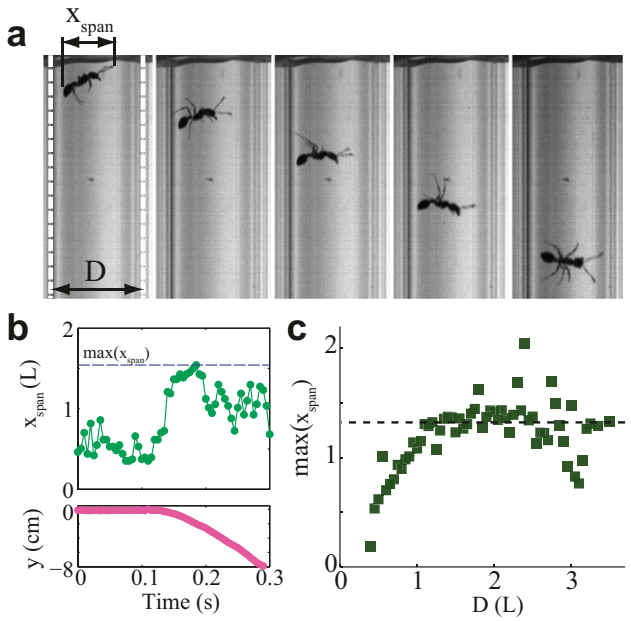

Fig. S14. Falling posture and arrest probability. (*A*) Five images from a perturbed fall. Images are separated by 10 ms. During perturbed falls we measured the total horizontal span of limbs, antennae, and body, called x_{span}. (*B*) x_{span} and vertical position, y, plotted versus time. Perturbation occurs at 0.1 s and vertical descent is accompanied by an increase in x_{span}. (*C*) Maximum lateral limb span [max(x_{span})] exhibited during fall as function of D(L). Limb span is constant above D > 1.3 L with max(x_{span}) = 1.33 ± 0.22 L (dashed line shown).

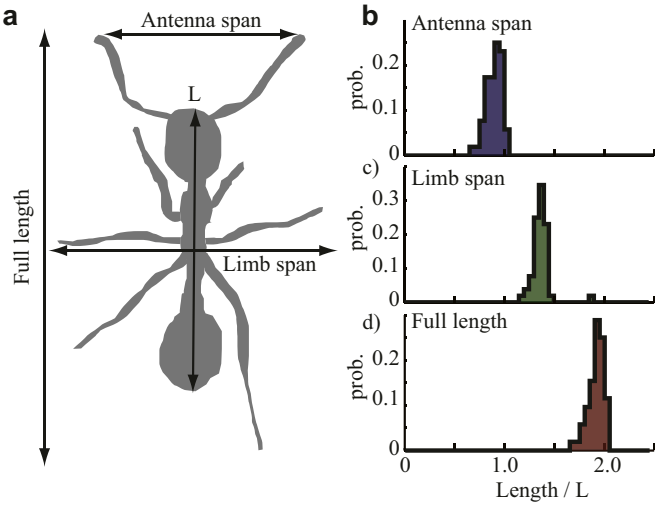

Fig. S15. Fire ant morphology data. This data is a reanalysis of the data reported from Tschinkel et al. (6) of morphogical measurements of the appendages and body segments of the fire ant *S. invicta*. (*A*) We measure the antennae span, the midlimb span, and the full-length distance defined as antenna length + head length + alinotum length + rear leg length. (*B–D*) Histograms of morphological measurements hypothesized to be relevant to tunnel arrest in units of body length.

Table S1. Distribution of particle size used in nest construction experiments

0–50 μm, roundness 80%		210–270 μm, roundness 80%		595–800 μm roundness 65%	
μm	%	μm	%	μm	%
>60	0	>420	0	>1,410	0
>50	2	>297	5	>841	5
>45	30	>210	85	>595	85
>35	60	>177	95	>250	95
>30	70				
<30	30				

We used collections of glass beads of diameter 50 μm (Jaygo Inc., Dragonite Glass beads 5210), 210 μm (Potters Industries Inc., Ballotini Impact beads, #6), or 595 μm (Potters Industries Inc., Ballotini Impact beads, #3). Rows indicate percentage of bulk mixture represented by that particle size or greater.

Table S2. Individual colony fit parameters for logistic fit of P_{arrest}

Colony	Fit (CI)
B	1.209 (1.167, 1.251)
C	1.56 (1.537, 1.583)
D	1.294 (1.263, 1.324)
E	1.485 (1.398, 1.572)
F	1.337 (1.274, 1.4)

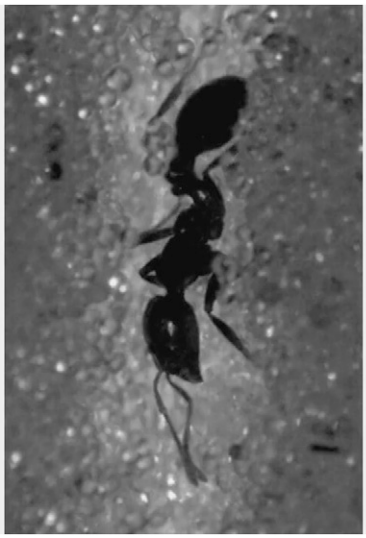

Movie S1. Rapid descent in an ant-constructed tunnel. The substrate consists of wetted 250 micron approximately spherical glass particles. Movie illustrates frequent contact of antennae with tunnel wall.

Movie S1

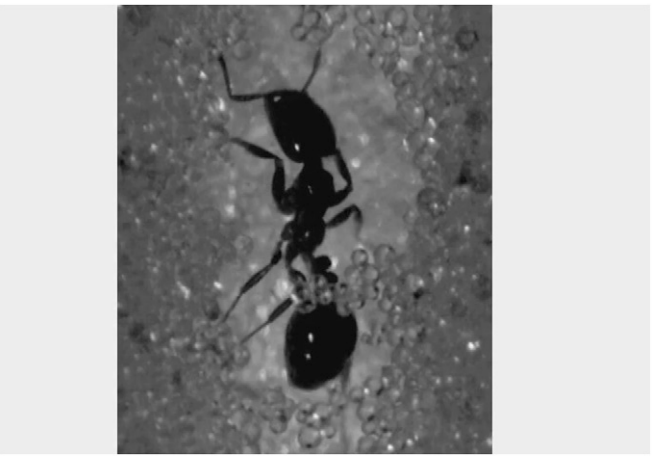

Movie S2. Rapid ascent in ant-constructed tunnel. The substrate consists of wetted 250 micron approximately spherical glass particles. During the middle of the climb, ant slips and falls backward but its motion is rapidly arrested.

Movie S2

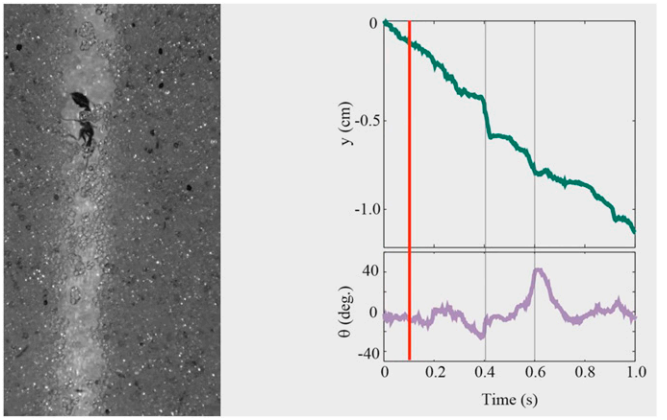

Movie S3. Rapid descent of an ant in an ant-constructed tunnel subject to two slip arrests. The substrate consists of wetted 250 micron approximately spherical glass particles. Tracked body position and orientation are shown with video and correspond to Fig. 3.

Movie S3

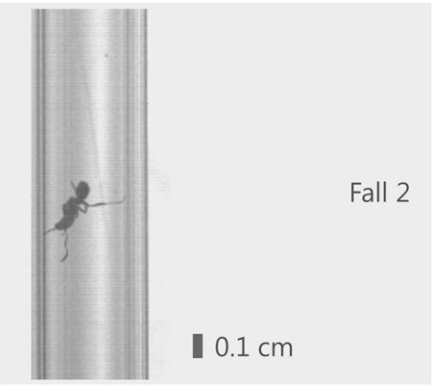

Movie S4. Nine slip arrests observed in glass tunnels of diameter D = 3–4 mm. All falls are headfirst and antennae are used as seventh and eighth limbs to arrest fall.

Movie S4

Movie S5. Movie illustrating perturbation experiment and stable and unstable falls.

Movie S5